COMMUNICATION

Check for updates

ZnX₂ mediated post-synthetic transformation of zero dimensional Cs₄PbBr₆ nanocrystals for opto-electronic applications†

Sumit Kumar Sharma,‡[a] Swati Mamgain,‡[b] Burhanuddin Attarwala[b] and Aswani Yella [ID] *[ab]

Herein we demonstrate a facile approach for the synthesis of all inorganic cesium lead halide perovskite nanocrystal composites CsPbX₃ (X = Cl, Br, I) with high quantum yield by post-synthetic modulation of zero dimensional Cs₄PbBr₆ nanocrystals with ZnX₂ salts. The transformation of Cs₄PbBr₆ nanocrystals into CsPbBr₃ takes place in two steps, the first step being the surface modification of the Cs₄PbBr₆ nanocrystals with Zn^{2+} ions and the second step being extraction of CsBr by the Zn^{2+} ions resulting in the formation of composite Cs₄PbBr₆/CsPbBr₃ nanocrystals. The transformed composite nanocrystals were found to have a PL QY exceeding 90% and the shape of the nanocrystals also changed from hexagonal to cubic shaped. Owing to the highly ionic nature of the nanocrystals, complete anion exchange could be also realized using ZnI₂ salt. In the case of the iodide post-treated samples, nanorods were obtained which exhibited bright red photoluminescence. Photodetectors based on the ZnI₂ treated Cs₄PbBr₆ NCs were fabricated, and the photodetectors exhibited a high on/off ratio with a fast response time. The excellent optoelectronic properties make this treatment versatile for a wide range of functional optoelectronic devices like light emitting diodes and photovoltaic devices.

Introduction

Lead halide perovskite NCs (especially CsPbX₃ where X = Cl, Br, I) have received massive attention in recent years as favorable optoelectronic materials due to their broad absorption,[1] intense photoluminescence (PL),[1] high photoluminescence (PL) quantum yield (QY),[2] very narrow emission line width,[3] high defect tolerance,[4] and wide-range band gaps which can be tuned by controlling the composition[5,6] and morphology.[7,8] Due to these interesting properties exhibited by the lead halide perovskite NCs they have been examined in the context of their use in optoelectronic devices, such as photovoltaics,[9,10] light emitting diodes,[11–15] lasers[16] and photodetectors.[17] In the recent past, numerous other types of cesium lead halide NCs, with structural dimensionality different from the three dimensional orthorhombic/cubic CsPbX₃ have gained a lot of attention.[18–25] The structural dimensionality in these structures depends on the extent of coupling of PbX₆ octahedra in the crystal. If all the corners of the lead hexahalide octahedra are shared, then they are electronically coupled in all three dimensions and referred to as 3D perovskites. If all the corners of the lead hexahalide octahedra are not shared, they are referred to as 0D perovskites.[25]

It is extensively recognized that the excellent optical properties in lead halide based perovskite materials come from the high defect tolerance.[4] Even the highly luminescent perovskite NCs prepared by the hot injection method are really not defect-free, and these defects serve as trapping centers for exciton recombination and decrease the photoluminescence quantum yields (PLQYs) of the NCs.[26–33] Different groups have recently synthesized 0D colloidal Cs₄PbBr₆ NCs and it has been found that these nanocrystals don't exhibit any photoluminescence.[25] However, the non-luminescent 0D Cs₄PbBr₆ NCs can be converted to 3D CsPbBr₃ NCs using additives like water,[34] PbBr₂[35] ligands,[36] and Prussian blue.[37] The non-luminescent nature of Cs₄PbBr₆ at room temperature is attributed to the origin of structural and point defects.[38] Nikl et al. observed the true emission of Cs₄PbBr₆ at low temperatures (4 K) and the true emission is centered at 375 nm. In the case of thin films at room temperature, Cs₄PbBr₆ is mixed with traces of the CsPbBr₃ phase, which in turn results in the emission at 545 nm. However in the case of nanocrystals, no emission has been observed so far for the pure Cs₄PbBr₆ nanocrystals.

Recently it has been shown that addition of appropriate metal halide salts significantly enhances the photoluminescence intensity of CsPbBr₃ nanocrystals by improving

[a]Centre for Research in Nanotechnology and Science, Indian Institute of Technology Bombay, 400076, India. E-mail: aswani.yella@iitb.ac.in

[b]Department of Metallurgical Engineering and Materials Science, Indian Institute of Technology Bombay, 400076, India

‡ Both the authors contributed equally.

the surface capping. Herein we demonstrate ZnX_2 mediated post-synthetic transformation of Cs_4PbBr_6 nanocrystals (NCs) into $CsPbX_3$ nanostructures through an intermediate composite $Cs_4PbX_6/CsPbX_3$. We find that this procedure results in a highly reproducible increase of the PL QY of up to 90% for the ZnX_2 treatment. The transformation takes place through the surface passivation of Cs_4PbBr_6 nanocrystals with ZnX_2 followed by anion exchange (in the case of ZnI_2 and $ZnCl_2$) resulting in the formation of an intermediate $Cs_4PbX_6@CsPbX_3$ passivated by ZnX_2 followed by the extraction of CsBr from the composite nanostructures. Interestingly, as soon the ZnX_2 is added to the nanocrystals, excitonic absorption resulting from the Cs_4PbBr_6 particles passivated with ZnX_2 is observed. This is the first time that the true emission of the Cs_4PbX_6 crystal structure in the nanocrystalline phase was observed at room temperature.

The Cs_4PbBr_6 nanocrystals were synthesized according to the hot injection strategy as described in the Experimental section. The Cs_4PbBr_6 nanocrystal dispersion in hexane is completely transparent and as shown in the TEM images in Fig. 1b–d, the pristine Cs_4PbBr_6 nanocrystals consist of hexagons of around 30 nm in size. The powder diffraction pattern indicated that the nanocrystals crystallized in the rhombohedral Cs_4PbBr_6 phase in the space group $R3c$.

The pristine Cs_4PbBr_6 nanocrystals (NCs) were post treated with a ZnX_2/hexane solution and used for further characterization. Upon addition of ZnX_2 (X= Cl, Br, I) solution, clear color change was observed (Fig. 2a). And the initially non-luminescent solution turned into a brightly luminescent solution under UV light after the post-treatment (Fig. 2b). To understand the reason for the observed color changes, powder diffraction analysis was carried out. Fig. 2c shows the X-ray diffraction patterns obtained for the pristine and ZnX_2 treated

NCs. The XRD pattern of the parent NCs indicated that they are crystalline and matched well with the reported rhombohedral Cs_4PbBr_6 phase. No characteristic reflections of $CsPbBr_3$, CsBr or $PbBr_2$ were observed. Upon treating with $ZnBr_2$, new reflections were observed along with the reflections from Cs_4PbBr_6. All the new reflections could be attributed to the $CsPbBr_3$ phase and the post treatment resulted in the formation of the composite $Cs_4PbBr_6/CsPbBr_3$. Similar behavior was observed in the case of ZnI_2 treated and $ZnCl_2$ treated NCs wherein a composite of $Cs_4PbX_6/CsPbX_3$ is formed. In the case of ZnI_2 treated NCs, the pristine Cs_4PbBr_6 reflections were shifted towards the lower 2θ indicating that anion exchange took place from the bromide to iodide resulting in the formation of Cs_4PbI_6. A slight shift towards higher 2θ was observed in the case of $ZnCl_2$ treated NCs. Interestingly, when the ZnX_2 post treated solutions were left without centrifugation for a few days, the luminescence of the solution was reduced in comparison to that of the samples which were centrifuged and washed after the ZnX_2 post-treatment. We have carried out XRD analysis on those samples left without centrifugation and Fig. 2d shows the diffraction patterns obtained for the same samples. From the diffraction patterns it can be seen that the $ZnBr_2$ left in the solution results in the complete transformation of 0D Cs_4PbBr_6 NCs into 3D $CsPbBr_3$ NCs. In the case of ZnI_2 post-treatment, the reflections from 0D Cs_4PbI_6 still exist, indicating that the transformation from 0D to 3D is not complete even after a few days.

The absorption spectra of the ZnX_2 treated Cs_4PbBr_6 NCs are shown in Fig. 3a. For the pristine nanocrystals, the absorption and the photoluminescence features are consistent with those in the previously reported studies. The absorption spectra of the as-prepared nanocrystals feature a strong and narrow absorption at 313 nm. The long tail in the absorption spectrum indicates that a certain degree of coupling exists between the $PbBr_6$ octahedra. Fig. 2a and b show the photographs of the pristine Cs_4PbBr_6 and ZnX_2 treated NCs under room light and UV light. Upon treating the NCs with the $ZnBr_2$/hexane solution, the initially colorless solution turned green color. The same is observed in the UV-vis absorption spectrum with a red shift of the absorption band edge to 510 nm. The features are similar to the characteristic feature of the 3D $CsPbBr_3$ NCs,[1–10] probably indicating the transformation of Cs_4PbBr_6 into $CsPbBr_3$ NCs. Along with this, another hump was observed at 420 nm in the $ZnBr_2$ treated sample. This hump was not observed previously in the pure $CsPbBr_3$ NCs,[1–10] the $ZnBr_2$ stabilized $CsPbBr_3$ NCs and the Zn^{2+} doped $CsPbBr_3$ nanocrystals.[39] To see if similar behavior is observed with other zinc halides, the Cs_4PbBr_6 NCs were also treated with ZnI_2 and $ZnCl_2$. $ZnCl_2$ treatment resulted in a slight blue shift in comparison to $ZnBr_2$ treated NCs. However, in the case of $ZnCl_2$ treated NCs, no hump in the absorption spectrum was evident. In the case of ZnI_2, an increased red shift (up to 670 nm) in comparison to that in the $ZnBr_2$ treatment was observed. Along with the red shifted absorption, a sharp peak at 550 nm can be seen.

To confirm if the peak observed at 420 nm arises from the sample, an aliquot of the Cs_4PbBr_6 NCs was taken in a cuvette, different concentrations of $ZnBr_2$ were added to the sample and

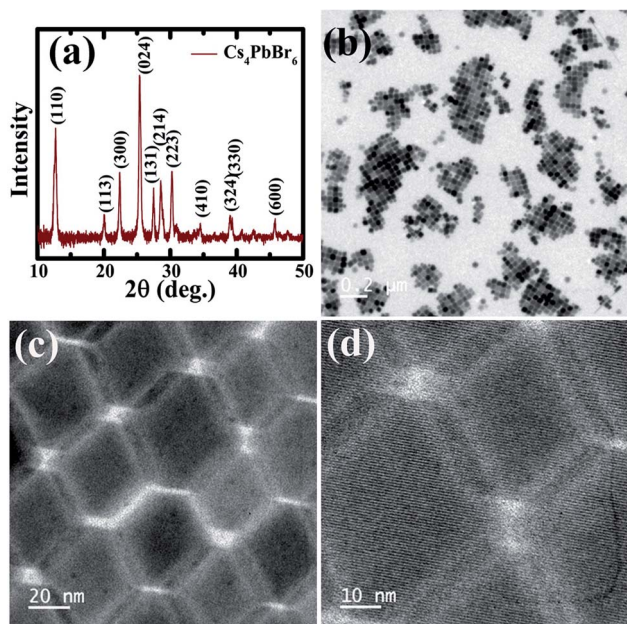Fig. 1 (a) X-ray diffraction patterns obtained of the pristine Cs_4PbBr_6 NCs. (b–d) TEM images of the pristine Cs_4PbBr_6 NCs at different magnifications.

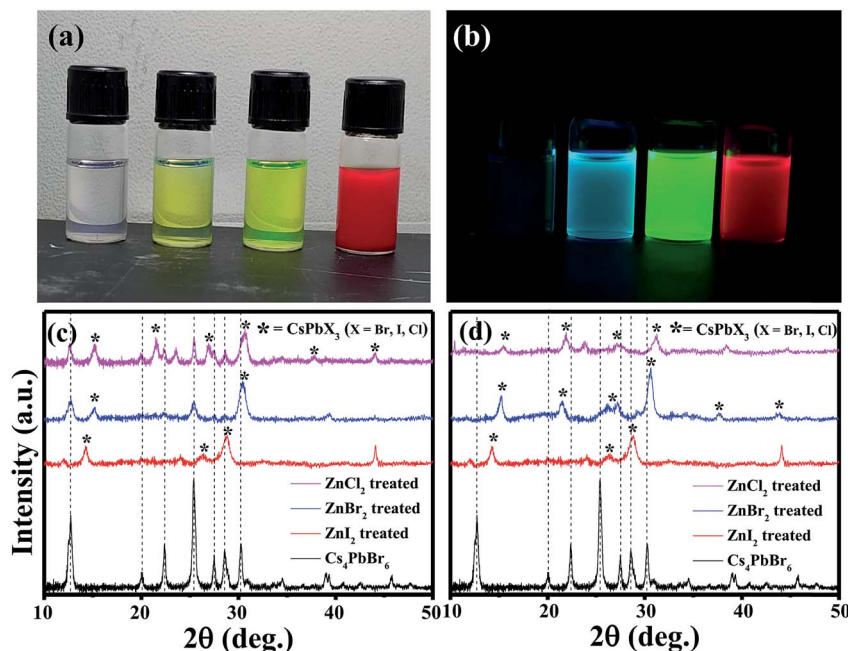Fig. 2 Photographs of the solutions of Cs_4PbBr_6, $ZnCl_2$ treated, $ZnBr_2$ treated and ZnI_2 treated NCs, respectively under ambient light (a) and under UV light (b). (c) X-ray diffraction patterns obtained for the pristine and ZnX_2 treated NCs. (d) X-ray diffraction patterns obtained of the samples left without centrifugation after the addition of ZnX_2.

the absorption spectrum of the $ZnBr_2$ treated NCs was measured. Fig. 3b shows the absorption spectra measured using different concentrations of the $ZnBr_2$/hexane solution added to the cuvette containing NCs. A sharp absorption peak at 425 nm along with a long tail extending up to 510 nm was observed. The absorption intensity of the tail increased gradually and a sharp band edge at 510 nm, which is a characteristic peak of $CsPbBr_3$, was observed. The peak at 425 nm is blue shifted to 420 nm and is masked (though visible) by the strong absorption of $CsPbBr_3$ in this region. Fig. S1† shows the comparison of the absorption spectra of the $CsPbBr_3$ nanocrystals synthesized and the $ZnBr_2$ treated Cs_4PbBr_6 NCs. A similar concentration dependent study was carried out in the case of ZnI_2 treated Cs_4PbBr_6 NCs. Fig. 3c shows the evolution of the absorption spectrum of ZnI_2 treated NCs with different amounts of ZnI_2 added. A sharp absorption at 540 nm is evident even with high amounts of added ZnI_2. $ZnBr_2$ treated NC samples were found to be highly stable even after 2 months of maintaining under 70% RH conditions. Fig. S2† shows photographs under UV light for the $ZnBr_2$ treated NC sample and the as-prepared CsPbBr3 NCs after storing under 70% RH conditions.

To corroborate the observed absorption behavior, photoluminescence (PL) studies were also carried out on the parent NCs and ZnX_2 treated NCs. Fig. 3d shows the PL spectra of the pristine NCs and $ZnBr_2$ treated NCs. No strong PL emission was observed, which is consistent with the previously observed decay of excitonic PL above temperatures of 100 K. Very weak PL emission centered at 515 nm was observed which can be attributed to the $CsPbBr_3$ phase embedded in the PL-inactive Cs_4PbBr_6 crystalline matrix. With the $ZnBr_2$ post-treated NC solution, strong PL was observed at 518 nm. From the literature,

it is known that the excitonic absorption peak of pure $CsPbBr_3$ NCs is located at around 510 nm. So, it is reasonable to speculate that the strong excitonic absorption peak and strong PL peak at 518 nm in Fig. 3d originate from the $CsPbBr_3$ NCs, indicating that a transformation might have taken place from Cs_4PbBr_6 to $CsPbBr_3$.

We also carried out $ZnBr_2$ concentration dependent emission studies. With the addition of $ZnBr_2$, two emission peaks were observed, one at 430 nm and the other at 510 nm, similar to the behavior observed in the absorption spectrum. The emission at 430 nm could be attributed to the 425 nm peak observed in the absorption spectrum and the peak at 510 nm could be attributed to the band edge emission corresponding to the absorption edge shown in Fig. 3e. Similar behavior was also observed in the case of the iodide counterpart, wherein the two emission peaks corresponds to the absorption peak at 550 nm and band edge absorption (Fig. 3f).

Together with the results obtained from the XRD studies and UV-vis and PL spectra, we speculate that $CsPbX_3$/Cs_4PbX_6 composites were formed after the post-treatment with ZnX_2. In the case of $ZnBr_2$, the excitonic $CsPbBr_3$ absorption was observed at 510 nm and the absorption peak observed at a lower wavelength could be attributed to the Cs_4PbBr_6 phase. It has been previously reported that defect states created due to the surface halide vacancies could be responsible for quenching the true emission in Cs_4PbBr_6 and were only observed at low temperatures (4 K). When the Zn^{2+} salts were added to the Cs_4PbBr_6 NCs, the surface halide defect states could be passivated and the true emission from the surface passivated/modified Cs_4PbBr_6 nanocrystals could be observed at 430 nm. The true emission of Cs_4PbBr_6 is observed for the first time at
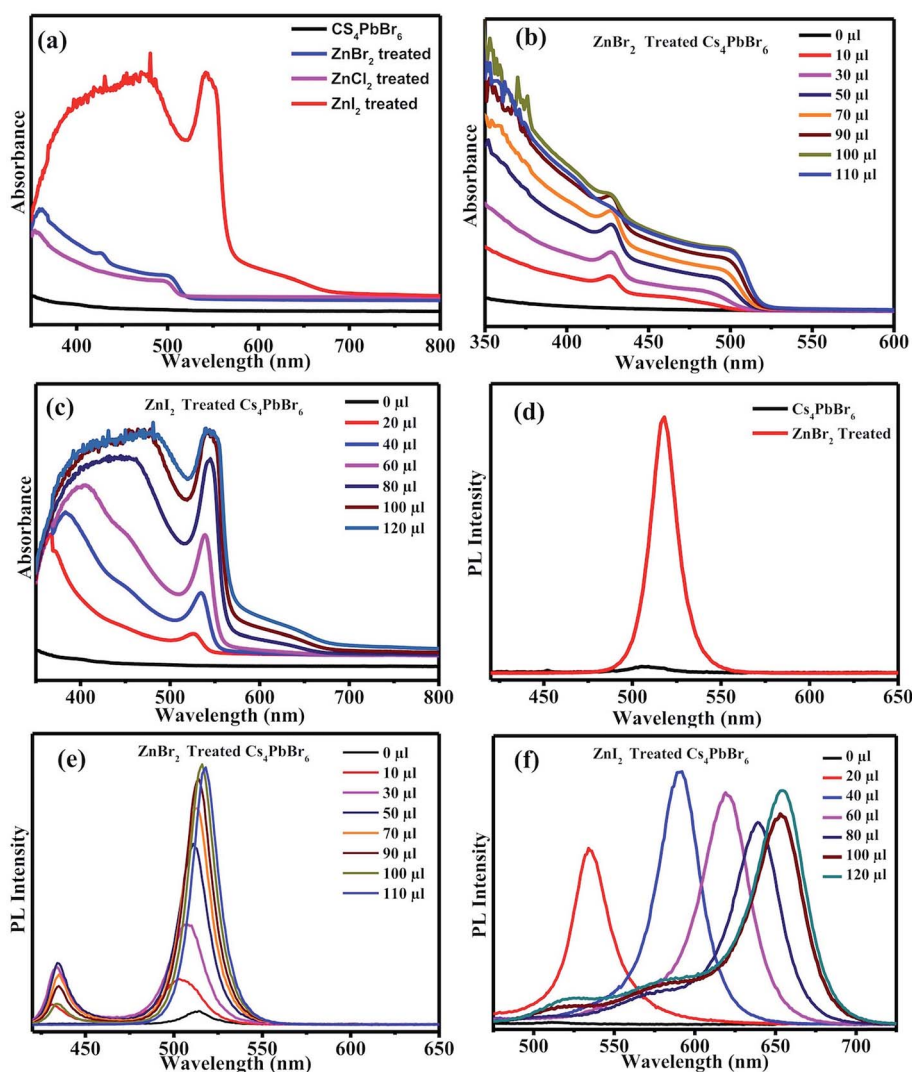
Fig. 3   (a) UV–vis absorption spectra of the ZnX_2 treated Cs_4PbBr_6 nanocrystals. (b) Absorption spectra measured using different concentrations of the $ZnBr_2$/hexane solution. (c) Absorption spectrum of ZnI_2 treated NCs with the different concentrations of the ZnI_2/hexane solution. (d) PL spectra of the pristine NCs and $ZnBr_2$ treated NCs. PL spectra of the Cs_4PbBr_6 NCs with different concentrations of (e) $ZnBr_2$ solution and (f) ZnI_2 solution.

room temperature when Zn^{2+} salts are used to passivate the surface defects; however, the Zn^{2+} salts also triggered the transformation of 0D Cs_4PbBr_6 NCs into 3D $CsPbBr_3$ NCs. So, the intensity of the true emission of Cs_4PbBr_6 NCs gradually decreased as the concentration of the zinc salt is increased. When the concentration of the zinc salt was kept constant at 50 μL of $ZnBr_2$, the intensity gradually decreased indicating that the whole process takes place through a two-step mechanism. Similar studies carried out using other salts like Cu^{2+} and Mn^{2+} didn't result in the enhancement of the PL QY. In the case of Mn^{2+} a slight increase was observed but Cu^{2+} didn't show any improvement in the PL QY. Fig. S3† shows the PL of the $CuBr_2$ and $MnBr_2$ treated Cs_4PbBr_6 NCs.

TEM images of the as-synthesized Cs_4PbBr_6 NCs show hexagonal shaped particles of around 30–35 nm in size similar to the particles reported previously. Fig. 4 shows the TEM images of the as-synthesized Cs_4PbBr_6 NCs and the $ZnBr_2$ treated samples.

When the samples were treated with 50 μL of $ZnBr_2$, initially hexagonal shaped particles were converted mostly to cubic shaped particles as shown in Fig. 4. More than 90% of the particles became cubic; however the cubic shaped particles did not have sharp edges as observed in the case of the as-prepared $CsPbBr_3$ NCs (Fig. S4†). The HR-TEM image (Fig. 4d) shows a lattice spacing of 0.58 nm for the (100) plane of $CsPbBr_3$ after $ZnBr_2$ treatment. The edges of the particles, however, show that the lattice spacing is not the same as that in the center of the particles. The lattice spacing of 0.33 nm for the (411) plane corresponds to the presence of Cs_4PbBr_6, indicating the formation of a composite of $CsPbBr_3/Cs_4PbBr_6$. A plausible two step formation mechanism can be inferred from the observed TEM images. As the Cs_4PbBr_6 nanocrystals were treated with the zinc halide salts, in the first step Zn^{2+} ions could passivate the surface of the nanocrystals and then result in the extraction of excess Cs^+ ions, and an increase in the dimensionality from 0D to 3D is
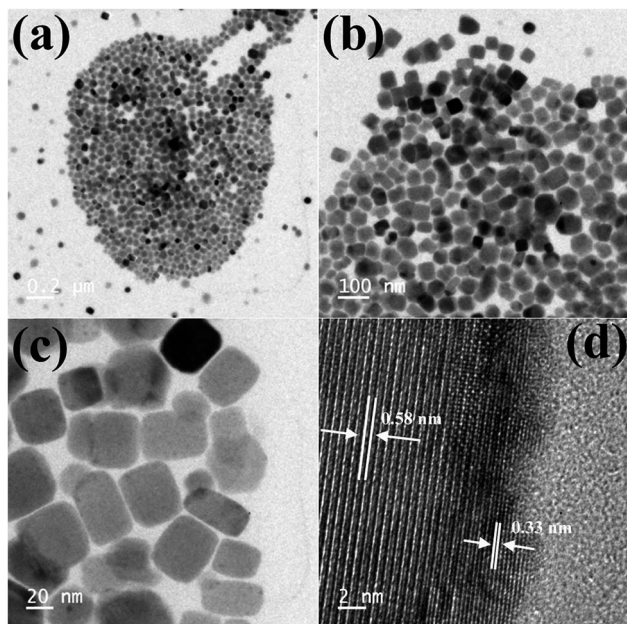
Fig. 4 TEM images of the ZnBr$_2$ treated Cs$_4$PbBr$_6$ NC samples (a–c) and HRTEM (d) image of the ZnBr$_2$ treated Cs$_4$PbBr$_6$ NC samples indicating the formation of a composite of CsPbBr$_3$/Cs$_4$PbBr$_6$ NCs.

observed. In the second step we believe that an inside out diffusion of Cs$^+$ ions takes place resulting in the formation of CsPbBr$_3$/Cs$_4$PbBr$_6$ composites.

When the Cs$_4$PbBr$_6$ NCs were treated with 40 μL of ZnI$_2$ solution, the shape of the particles changed from hexagonal to rod shaped. As seen in the TEM images shown in Fig. 5b the corners of the rods still have hexagonal facets. With the increase in the concentration of the ZnI$_2$ solution to 100 μL the length of the rods increased to nearly 250 nm and the width increased to 20–30 nm.

To see if any zinc is present on the surface of the nanocrystals, resulting in the enhanced PL QY, X-ray photoelectron spectroscopy (XPS) measurements have been used to assess the surface modification of the NCs and to understand the mechanism of PL enhancement. After measurements, all core level spectra were calibrated using the C 1s peak at 285.0 eV. The high-resolution XPS spectrum of untreated NCs for Pb 4f yields 2 peaks as shown in Fig. S5.† Two intense peaks are observed at 138 eV (4f$_{7/2}$) and 143 eV (4f$_{5/2}$) with a spin–orbit splitting of nearly 5 eV, which corresponds to Pb in the 2+ oxidation state. Quantitative XPS analysis indicates that Cs : Pb : Br = 1.5 : 1 : 4.2 for untreated Cs$_4$PbBr$_6$ NCs, which is Pb rich in composition. However, for ZnBr$_2$-Cs$_4$PbBr$_6$ NCs, the composition becomes anion-rich (Cs : Pb : Br = 0.6 : 1 : 5.5), which was also repeatedly observed (Fig. S6†). A small fraction of the Zn^{2+} was also observed in the ZnBr$_2$ treated Cs$_4$PbBr$_6$ NCs, with the ratio of Pb : Zn = 1 : 0.08. This also conforms with the previous observations that the Zn^{2+} ions modify the surface of the nanocrystals, which then results in the extraction of excess Cs$^+$ ions from the Cs$_4$PbBr$_6$ NCs. Furthermore, the Pb/Cs ratio increased from 0.66 to 1.66 in ZnBr$_2$ treated Cs$_4$PbBr$_6$ NCs compared with pristine-Cs$_4$PbBr$_6$ NCs indicating that ZnBr$_2$ extracted excess Cs$^+$ ions present. This is also consistent with the XRD analysis wherein the Cs$_4$PbBr$_6$ is converted to CsPbBr$_3$ after the extraction of cesium ions. We have also carried out XPS analysis of the ZnI$_2$ treated Cs$_4$PbBr$_6$ NCs and found that the ratio of Pb : Zn (1 : 0.15) is much higher compared to that in the bromine case (Fig. S7†).

Owing to the one-dimensional nature of the nanorods in the case of ZnI$_2$ treated Cs$_4$PbBr$_6$ NCs, we have explored their potential application in optoelectronic devices. To this end, we have fabricated photodetectors by dropcasting the ZnI$_2$ treated NCs in hexane between two fluorine doped tin oxide (FTO)

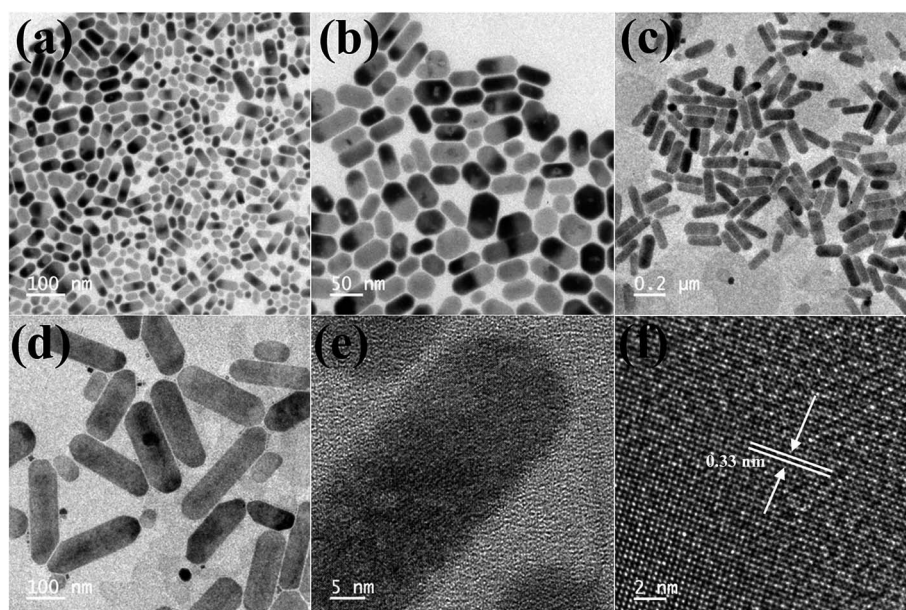**Fig. 5** TEM images obtained after the 40 μL ZnI$_2$ post treatment (a and b) and 100 μL ZnI$_2$ post treatment (c–f). HRTEM images showing the lattice spacing after the post treatment with 100 μL ZnI$_2$ (e and f).

electrodes. Fig. 6a shows the schematic of the device architecture that is employed for the fabrication of the devices. The dark current observed was in the order of a few picoamperes, within the detection limit of our instrument. The current of the same device increased under illumination using a diode source of 617 nm, demonstrating their potential as an efficient photodetector. Fig. 6b shows the IV curves obtained in the dark and in the presence of the light diodes. The ratio of the photocurrent to dark current could reach over two orders of magnitude. Time-dependent photocurrent measurements were carried out by pulsing the diode at a fixed light intensity with an applied bias voltage of 2 V. Prompt and reproducible photocurrent response to the pulsing was observed indicating the excellent optical switching and stability of the photodetectors. The rise time and decay time were also determined from the pulsing experiments and they are in the order of a few milliseconds as shown in Fig. 6d. When the photodetectors were fabricated using $ZnBr_2$ treated nanocrystals, the currents obtained were lower compared to those using the ZnI_2 treated samples. Fig. S8† shows the performance of the photodetectors using $ZnBr_2$ treated NCs in the same configuration. This indicates that the performance of the photodetectors could be improved if the length of the nanorods could be made longer than the width of the channel used and also by removing the surface capping ligands by appropriate treatments.

In conclusion, we have developed a simple and convenient post synthetic strategy for the transformation of 0D Cs_4PbBr_6 into highly luminescent $CsPbBr_3/Cs_4PbBr_6$ composites using $ZnBr_2$ treatment. The transformation with $ZnBr_2$ treatment proceeds through a two-step process, where in the first step, zinc doped/modified Cs_4PbBr_6 NCs are formed which then results in the conversion to $CsPbBr_3/Cs_4PbBr_6$ nanocomposites. The composite of $CsPbBr_3/Cs_4PbBr_6$ NCs is found to be very

highly luminescent with a PL QY of 90%. In the case of ZnI_2 treatment, the post synthetic treatment also resulted in morphological transformation from the hexagonal shaped nanocrystals to nanorods. The length of the rods could be varied depending on the concentration of the nanocrystals and the zinc iodide salt added. In both the iodide and bromide case an intermediate is formed upon treatment with the zinc salt. The intermediate was observed in the time/concentration dependent UV-vis and PL studies, and from the X-ray diffraction analysis, we presume that it is the 0D structure modified/doped by the zinc cations. Photodetectors based on the ZnI_2 treated Cs_4PbBr_6 NCs were fabricated, which exhibit a high on/off ratio with a fast response time. The excellent optoelectronic properties make this treatment versatile for a wide range of functional optoelectronic devices like light emitting diodes and photovoltaic devices.

Experimental section

Chemicals

Cesium carbonate (Cs_2CO_3, 99.9%), lead(II) bromide (98%), zinc(II) iodide (98%), zinc(II) chloride (99%), oleylamine (OLA, 70%), oleic acid (90%), and 1-octadecene (90%) were purchased from Sigma Aldrich. Zinc(II) bromide (98%) was purchased from Alfa Aesar.

Synthesis of cesium oleate

Cesium carbonate (Cs_2CO_3, 160 mg), oleic acid (1 mL), and octadecene (16 mL) were added to a three-neck flat bottom flask and kept under vacuum for 30 min at 120 °C. After 30 minutes the temperature was increased to 150 °C and the system was
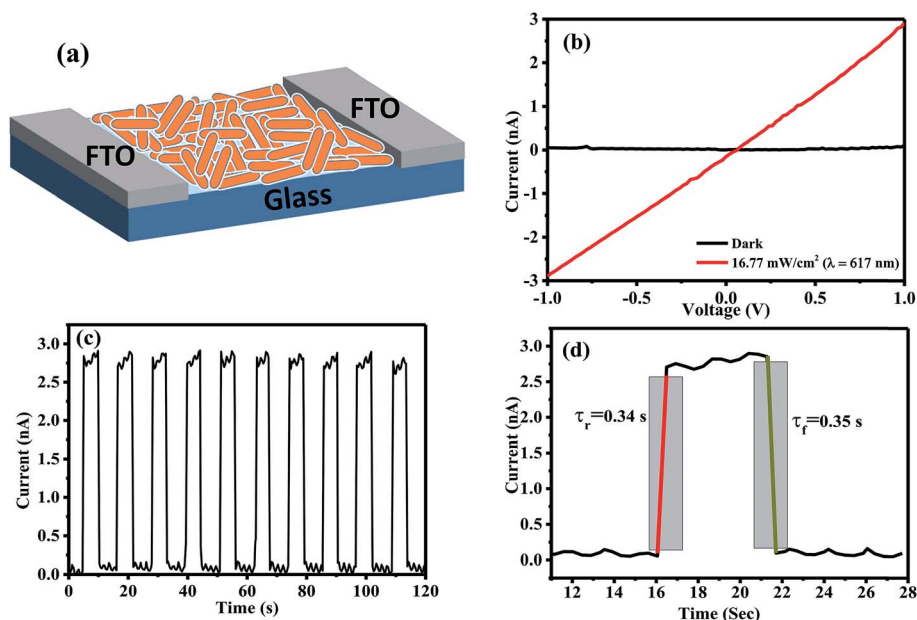

Fig. 6 (a) Schematic of the photo-detector architecture. (b) $I-V$ curves in the dark and in the presence of 617 nm light. (c) Photocurrent time characteristics of the photo detector in the dark and under light (617 nm, 1 volt). (d) Rise and decay time.

kept under a N_2 atmosphere until a clear solution of cesium oleate was obtained.

Synthesis of Cs_4PbBr_6 nanoparticles

Octadecene (10 mL), oleylamine (1 mL), oleic acid (1 mL) and lead bromide (0.36 mmol, 73.4 mg) were loaded into a three-neck round bottom flask and degassed for 30 min at 120 °C. The flask was then filled with N_2 and the temperature was increased to 140 °C. After that, 4.4 mL of hot cesium oleate solution was injected quickly. After 5 s, the reaction mixture was quenched in an ice-water bath.

Synthesis of $CsPbBr_3$ nanoparticles

Lead bromide (207 mg) and octadecene (15 mL) were loaded into a three-neck round bottom flask and degassed for 1 hour at 120 °C. The flask was then filled with N_2 and oleylamine (1.5 mL) and oleic acid (1.5 mL) were added. After complete solubilisation of $PbBr_2$, the temperature was increased to 165 °C and finally the as-prepared Cs-oleate (1.2 mL) was injected. The reaction was immediately quenched in an ice-water bath.

Purification of nano particles

The crude solution of nanoparticles was first centrifuged at 6000 rpm for 10 min. After that, the supernatant was discarded and the precipitate was redispersed in hexane solution. Then again, the large particles present in the solution were removed by centrifugation at 6000 rpm for 10 min. The supernatant was discarded and a colloidal solution of nanoparticles was obtained in hexane.

ZnX_2 (X = Br, I and Cl) treatment

The NCs dispersed in hexane ($\sim$8 mg mL^{-1}) were treated with the pre-made zinc halide solution. Zinc halide solutions were prepared by dissolving zinc halides (ZnX_2, X= I, Br, Cl) (0.05 M) in the mixture of hexane (2 mL) and oleylamine (40 μL) at room temperature. Then the required zinc halide solution was added to 1 mL of the Cs_4PbBr_6 NCs in hexane solution (8 mg mL^{-1}) under constant stirring. Excess zinc halide salts are removed by centrifugation and the NCs can be stored in organic solvents like hexane, toluene, etc. for a few months.

Characterization

High resolution transmission electron microscope images were obtained using a Tecnai G2 F30 300 kV transmission electron microscope. X-ray diffraction spectra were obtained by using a Rigaku Japan SmartLab X-ray diffractometer (Cu Kα, λ = 1.541). PL spectra were collected by using a Horiba FluoroMax spectrometer with 400 nm excitation wavelength, while UV-vis absorption measurement was performed using a UV-vis-NIR spectrometer (PerkinElmer LAMBDA 950). The room-temperature PLQY was calculated according to the following equation[38]

$$QY_{sample} = QY_{ref} \left(\frac{PLArea_{sample}}{PLArea_{ref}} \right) \left(\frac{I_{ref}}{I_{sample}} \right) \left(\frac{n_{sample}^2}{n_{ref}^2} \right)$$

In this equation, QY_{sample} is the PLQY of the sample. $PLArea_{sample}$ is the integrated emission spectrum curve area for the sample. I_{sample} is the absorption value at the excitation wavelength for the sample. n_{sample} is the refractive index of the employed solvent. QY_{ref}, $PLArea_{ref}$, I_{ref} and n_{ref} are those for the standard reference respectively. In our experiment, fluorescein sodium salt in water and Rhodamine 6G in water (PLQY = 0.95) were chosen to be the standards for green and red spectral regions and the standard solutions should be freshly prepared. Attention was paid to keeping the optical densities of the sample and standard below 0.1 at the excitation wavelength.

Photodetector fabrication

Laser patterned FTO coated glass with an etched area was used as the photodetector. Before deposition, the laser patterned FTO was cleaned thoroughly by using a soap solution, DI water, acetone, and ethanol for 10 minutes, respectively, by ultrasonication. Perovskite nanocrystals in hexane were drop cast on the etched area of the FTO coated glass by masking the unetched area with scotch tape. The drop cast substrate was then subjected to vacuum drying. Then the photoresponse was measured under a 617 nm LED light.

Conflicts of interest

There are no conflicts to declare.

Acknowledgements

References

1 L. Protesescu, S. Yakunin, M. I. Bodnarchuk, F. Krieg, R. Caputo, C. H. Hendon, R. X. Yang, A. Walsh and M. V. Kovalenko, *Nano Lett.*, 2015, **15**, 3692–3696.

2 A. Swarnkar, R. Chulliyil, V. K. Ravi, M. Irfanullah, A. Chowdhury and A. Nag, *Angew. Chem.*, 2015, **127**, 15644–15648.

3 R. E. Brandt, V. Stevanović, D. S. Ginley and T. Buonassisi, *MRS Commun.*, 2015, **5**, 265–275.

4 D. N. Dirin, L. Protesescu, D. Trummer, I. V. Kochetygov, S. Yakunin, F. Krumeich, N. P. Stadie and M. V. Kovalenko, *Nano Lett.*, 2016, **16**, 5866–5874.

5 Q. A. Akkerman, V. D'Innocenzo, S. Accornero, A. Scarpellini, A. Petrozza, M. Prato and L. Manna, *J. Am. Chem. Soc.*, 2015, **137**, 10276–10281.

6 G. Nedelcu, L. Protesescu, S. Yakunin, M. I. Bodnarchuk, M. J. Grotevent and M. V. Kovalenko, *Nano Lett.*, 2015, **15**, 5635–5640.

7 Y. Bekenstein, B. A. Koscher, S. W. Eaton, P. Yang and A. P. Alivisatos, *J. Am. Chem. Soc.*, 2015, **137**, 16008–16011.

8 D. Zhang, Y. Yu, Y. Bekenstein, A. B. Wong, A. P. Alivisatos and P. Yang, *J. Am. Chem. Soc.*, 2016, **138**, 13155–13158.

9 A. Swarnkar, A. R. Marshall, E. M. Sanehira, B. D. Chernomordik, D. T. Moore, J. A. Christians, T. Chakrabarti and J. M. Luther, *Science*, 2016, **354**, 92–95.

10 Q. A. Akkerman, M. Gandini, F. Di Stasio, P. Rastogi, F. Palazon, G. Bertoni, J. M. Ball, M. Prato, A. Petrozza and L. Manna, *Nat. Energy*, 2017, **2**, 16194.

11 X. Zhang, H. Lin, H. Huang, C. Reckmeier, Y. Zhang, W. C. H. Choy and A. L. Rogach, *Nano Lett.*, 2016, **16**, 1415–1420.

12 H. Huang, H. Lin, S. V. Kershaw, A. S. Susha, W. C. H. Choy and A. L. Rogach, *J. Phys. Chem. Lett.*, 2016, **7**, 4398–4404.

13 F. Palazon, F. Di Stasio, Q. A. Akkerman, R. Krahne, M. Prato and L. Manna, *Chem. Mater.*, 2016, **28**, 2902–2906.

14 X. Li, Y. Wu, S. Zhang, B. Cai, Y. Gu, J. Song and H. Zeng, *Adv. Funct. Mater.*, 2016, **26**, 2435–2445.

15 J. Song, J. Li, X. Li, L. Xu, Y. Dong and H. Zeng, *Adv. Mater.*, 2015, **27**, 7162–7167.

16 Y. Wang, X. Li, J. Song, L. Xiao, H. Zeng and H. Sun, *Adv. Mater.*, 2015, **27**, 7101–7108.

17 P. Ramasamy, D.-H. Lim, B. Kim, S.-H. Lee, M.-S. Lee and J.-S. Lee, *Chem. Commun.*, 2016, **52**, 2067–2070.

18 X. Zhang, B. Xu, J. Zhang, Y. Gao, Y. Zheng, K. Wang and X. W. Sun, *Adv. Funct. Mater.*, 2016, **26**, 4595–4600.

19 K.-H. Wang, L. Wu, L. Li, H.-B. Yao, H.-S. Qian and S.-H. Yu, *Angew. Chem., Int. Ed.*, 2016, **55**, 8328–8332.

20 G. Li, H. Wang, Z. Zhu, Y. Chang, T. Zhang, Z. Song and Y. Jiang, *Chem. Commun.*, 2016, **52**, 11296–11299.

21 M. I. Saidaminov, J. Almutlaq, S. Sarmah, I. Dursun, A. A. Zhumekenov, R. Begum, J. Pan, N. Cho, O. F. Mohammed and O. M. Bakr, *ACS Energy Lett.*, 2016, **1**, 840–845.

22 D. Chen, Z. Wan, X. Chen, Y. Yuan and J. Zhong, *J. Mater. Chem. C*, 2016, **4**, 10646–10653.

23 Q. A. Akkerman, S. Park, E. Radicchi, F. Nunzi, E. Mosconi, F. De Angelis, R. Brescia, P. Rastogi, M. Prato and L. Manna, *Nano Lett.*, 2017, **17**, 1924–1930.

24 J. Kang and L.-W. Wang, *J. Phys. Chem. Lett.*, 2017, **8**, 489–493.

25 S. Seth, N. Mondal, S. Patra and A. Samanta, *J. Phys. Chem. Lett.*, 2016, **7**, 266–271.

26 J. Y. Woo, Y. Kim, J. Bae, T. G. Kim, J. W. Kim, D. C. Lee and S. Jeong, *Chem. Mater.*, 2017, **29**, 7088–7092.

27 N. K. Noel, A. Abate, S. D. Stranks, E. S. Parrott, V. M. Burlakov, A. Goriely and H. J. Snaith, *ACS Nano*, 2014, **8**, 9815–9821.

28 F. Di Stasio, S. Christodoulou, N. Huo and G. Konstantatos, *Chem. Mater.*, 2017, **29**, 7663–7667.

29 B. A. Koscher, J. K. Swabeck, N. D. Bronstein and A. P. Alivisatos, *J. Am. Chem. Soc.*, 2017, **139**, 6566–6569.

30 J. Pan, Y. Shang, J. Yin, M. De Bastiani, W. Peng, I. Dursun, L. Sinatra, A. M. El-Zohry, M. N. Hedhili, A.-H. Emwas, O. F. Mohammed, Z. Ning and O. M. Bakr, *J. Am. Chem. Soc.*, 2018, **140**, 562–565.

31 G. Rainò, G. Nedelcu, L. Protesescu, M. I. Bodnarchuk, M. V. Kovalenko, R. F. Mahrt and T. Stöferle, *ACS Nano*, 2016, **10**, 2485–2490.

32 L. Wu, H. Hu, Y. Xu, S. Jiang, M. Chen, Q. Zhong, D. Yang, Q. Liu, Y. Zhao, B. Sun, Q. Zhang and Y. Yin, *Nano Lett.*, 2017, **17**, 5799–5804.

33 Z. Liu, Y. Bekenstein, X. Ye, S. C. Nguyen, J. Swabeck, D. Zhang, S.-T. Lee, P. Yang, W. Ma and A. P. Alivisatos, *J. Am. Chem. Soc.*, 2017, **139**, 5309–5312.

34 F. Palazon, G. Almeida, Q. A. Akkerman, L. De Trizio, Z. Dang, M. Prato and L. Manna, *Chem. Mater.*, 2017, **29**, 4167–4171.

35 F. Palazon, C. Urso, L. De Trizio, Q. Akkerman, S. Marras, F. Locardi, I. Nelli, M. Ferretti, M. Prato and L. Manna, *ACS Energy Lett.*, 2017, **2**, 2445–2448.

36 M. Nikl, E. Mihokova, K. Nitsch, F. Somma, C. Giampaolo, G. P. Pazzi, P. Fabeni and S. Zazubovich, *Chem. Phys. Lett.*, 1999, **306**, 280–284.

37 W. van der Stam, J. J. Geuchies, T. Altantzis, K. H. W. van den Bos, J. D. Meeldijk, S. Van Aert, S. Bals, D. Vanmaekelbergh and C. de Mello Donega, *J. Am. Chem. Soc.*, 2017, **139**, 4087–4097.

38 H. Duan, Y. Jiang, Y. Zhang, D. Sun, C. Liu, J. Huang, X. Lan, H. Zhou, L. Chen and H. Zhong, *Nanotechnology*, 2013, **24**, 285201.

39 W. Stam, J. J. Geuchies, T. Altantzis, K. H. W. van den Bos, J. D. Meeldijk, S. Van Aert, S. Bals, D. Vanmaekelbergh and C. de Mello Donega, *J. Am. Chem. Soc.*, 2017, **139**, 4087–4097.